2023 22nd IEEE Intersociety Conference on Thermal and Thermomechanical Phenomena in Electronic Systems (ITherm) | 979-8-3503-2166-1/23/$31.00 ©2023 IEEE | DOI: 10.1109/ITHERM55368.2023.10177590

Hotspot-targeted Cooling Scheme with Hybrid Jet Impingement/Thermal Through Silicon Via (TSV)

Shuhang Lyu[1], Qianying Wu[2], Tiwei Wei[1,*]
1. School of Mechanical Engineering, Purdue University, West Lafayette, IN 47907
2. Department of Mechanical Engineering, Stanford University, Stanford, CA 94305
*Corresponding email: tiwei@purdue.edu

***Abstract*—With continuous miniaturization of electronic devices, the system complexity and power density increase rapidly, causing localized high heat flux on chips. Hotspot-targeted thermal management has attracted extensive interest due to the concerns about chip performance and reliability. In this work, we proposed a hotspot-targeted hybrid cooling scheme that integrates jet impingement cooling with thermal TSVs. The cooling solution creates a heat transfer route for the hotspot heat flux by combining the high HTC in the stagnation region of jet impingement and superior heat conduction of thermal TSVs. The cooling performance of the scheme is benchmarked by performing CFD simulations. The proposed solution shows a remarkable 54% improvement in temperature uniformity and a significant 20% reduction of temperature rise compared to three other reference cooling solutions, including uniform cooling and stand-alone thermal TSV or impingement jet cooling scheme. In this paper, we investigate the impact of the TSV diameter, shape and TSV density to enhance the cooling performance. Firstly, the TSV dimensions are optimized to reduce occupied routing space. An optimal TSV diameter is obtained, which maintains a low overall thermal resistance and well confines the heat spreading in bulk TSV. Furthermore, we present a design with an exposed TSV array, which could enhance the local HTC in the hotspot region by aligning a protruded TSV array to the impingement jet. The TSV array with an optimal array density is demonstrated to be capable of effectively reducing temperature non-uniformity and peak temperature.**

Keywords—hotspot, thermal management, thermal through silicon via, impingement jet cooling, temperature uniformity, surface enhancement, CFD simulation

I. INTRODUCTION

As transistors continuously scale down, thermal management has become a major concern for the design of microelectronics [1]. Recent advances in the miniaturization of electronic devices and the complexity of systems are causing localized high heat flux, which can achieve more than 1000 W/cm^2 [2]. The concentrated high heat flux can render specific regions with peak temperatures known as hotspots. The temperature rises at hotspots bring about non-uniformity of temperature distribution along chip interfaces, which significantly degrades the performance and reliability of devices [3]. Hotspot-targeted cooling techniques have attracted extensive research interest due to the importance of hotspot thermal management in microelectronics design.

With the existence of hotspots, the heat flux can be quite non-uniform across the chip heat source regions. Conventional cooling solutions with a uniform heat transfer coefficient (HTC) distribution cause overcooling of the background region and undercooling of the hotspot region, leading to intensive energy consumption and notable temperature non-uniformity [3]. Therefore, advanced cooling solutions should be developed to eliminate the hotspots. In the literature, many hotspot-targeted cooling solutions have been proposed to reduce the temperature rise at hotspots, such as thermoelectric coolers (TEC) [4], micro heat pipes [5], heat spreaders with high thermal conductivity materials, such as graphene [6] and diamond [7], digital-microfluidic embedded cooling [8], microchannel cooling [3], [9], [10], and impingement jet cooling [11].

One of the most popular approaches to reducing the temperature rise of hotspots is creating a non-uniform HTC distribution to accommodate the non-uniformity of heat flux on the chip heat source region. Various approaches have been applied to address the high heat flux with an enhanced heat transfer in the hotspot regions. Small-sized TEC has shown great potential in dealing with hotspots as they can be integrated with integrated circuit (IC) processing and directly attached to hotspot regions, rendering a localized heat transfer enhancement and thus a decrease in temperature rise [2]. TEC is a kind of solid-state cooler that offers a reliable and low-noise cooling solution, but the additional energy consumption and low energy efficiency are the main drawbacks of TEC [4]. Topology optimization can be utilized to control the flow characteristics in microchannels and thus achieve desired HTC distribution. For example, Sharma et al. [3], [9] optimized the design of microchannels to create a non-uniform HTC that accommodates the heat flux distribution on the chip interface. Moreover, liquid cooling with surface enhancement has been proven promising hotspot-targeted approaches as they can locally enhance convective heat transfer in hotspot regions. It has been demonstrated that micro-fins [12] and porous media [13] can be embedded in microfluidic cooling solutions to strengthen heat transfer and alleviate the temperature rise in hotspot regions.

Among these cooling schemes, impingement jet cooling has shown distinctive advantages due to the non-uniform nature of HTC distribution on the target surface of the microjet [11], [14]. In impingement jet cooling, the boundary layer grows with the distance from the inlet nozzle, leading to a decrease of HTC

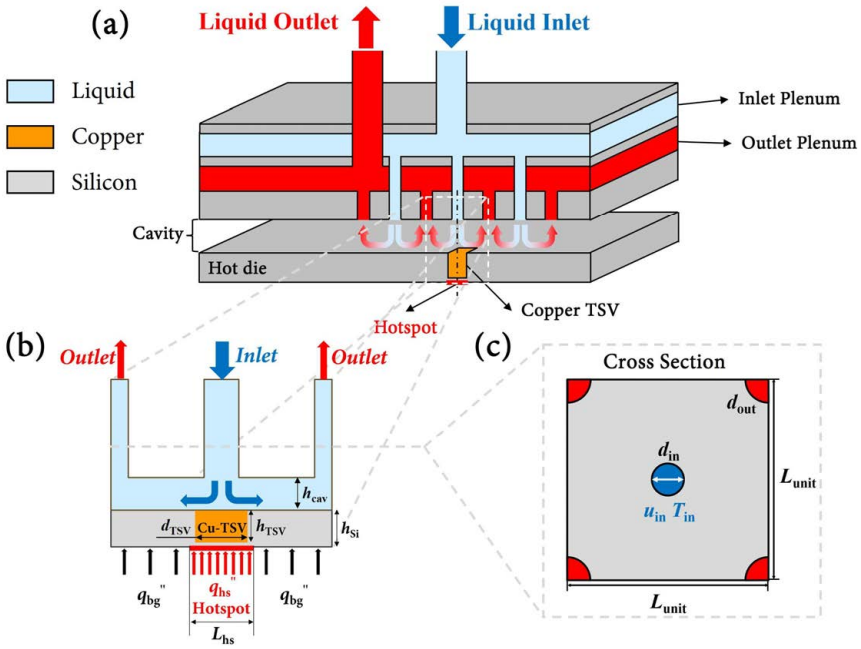

Fig. 1. Configuration of hybrid jet impingement/Thermal TSV cooling solution. The inlet nozzle, thermal TSV, and hotspot are horizontally aligned to create a heat transfer route for the high heat flux in the hotspot region. (a) Schematic of the cooling solution with an $N\times N$ nozzle array. (b) A unit cell of the jet array cooler. (c) Cross-sectional view of the unit cell with a single inlet and four outlets.

along the radial direction [15]. Thus, the target surface can be divided into three regions, the high-HTC stagnation region right below the nozzle, and the low-HTC wall jet and decay regions away from the nozzle [11]. The heat transfer enhancement in the stagnation region can be used to dissipate the high heat flux from hotspots and enhance temperature uniformity if the nozzles are well aligned with the hotspots. The demonstration of a hotspot-targeted jet cooler directly on the silicon die backside is achieved by Wei et al [11]. They designed and fabricated a 3D-printed jet cooler that aligns the inlet nozzles with hotspots on a testing chip. The cooler showed superior performance in maintaining a uniform temperature on the chip interface. However, the jet cooling performance on the hotspots is still limited by the heat spreading resistance through the silicon thickness.

Thermal Through Silicon Via (TSV) is thermal metal via fabricated in silicon dies to facilitate vertical heat transfer in 3D ICs [16], [17]. Compared to signal vias, thermal TSVs are dummy vias made of materials with high thermal conductivity and thus can increase the effective thermal conductivity of dies. Thermal TSVs can be arranged specifically near hotspots to reduce the peak temperature [16]. Although thermal TSVs can significantly decrease thermal resistance, they occupy valuable routing space and increase the distance between IC blocks [17]. Therefore, the design of thermal TSVs should be optimized to achieve a minimum usage of additional space while maintaining a predominant effect on heat transfer.

In this work, we propose a design of a hotspot-targeted impingement jet cooling solution with embedded thermal TSVs on the chip backside. By aligning the hotspots, inlet nozzles, and thermal TSVs, we create a heat transfer route with extraordinarily low thermal resistance for the high heat flux generated in the hotspot region. The cooling performance of the design is benchmarked by evaluating the overall thermal resistance and the temperature uniformity of the chip interface in Computational Fluid Dynamics (CFD) simulations and compared with other cooling solutions. The effects of dimensions and shapes of thermal TSVs are investigated to obtain the optimal design with minimum occupied space of thermal TSVs. Moreover, we demonstrate that the thermal resistance can be further reduced by fabricating a thermal TSV array and exposing TSVs as micro-fins. The effects of array density are studied to obtain optimal cooling performance.

II. Methodology

A. Model Geometry and Parameters

The design of the hybrid jet impingement/Thermal TSV cooling solution is shown in Fig. 1. Deionized (DI) water is chosen as the coolant here. The jet cooler consists of $N\times N$ inlet nozzle arrays and $(N+1) \times (N+1)$ outlet nozzles. A unit cell of the jet array cooler is shown in Fig.1b. The coolant will first flow into the inlet plenum from a single fluid inlet and then be distributed into an array of circular nozzles designed near the hotspot region. The jet flows through the inlet nozzles and impinges the die surface to dissipate the hotspots with high heat flux through convection cooling. The fluid will then be collected to the outlet plenum with the help of a distributed return microchannels architecture. A circular copper TSV is fabricated in the silicon die and aligned with the hotspot to enhance vertical heat transfer in the hotspot region. One of the inlet nozzles is also aligned with the hotspot and the TSV, which utilizes the high HTC in the stagnation region of the impingement jet to facilitate heat dissipation from the hotspot. Thus, an efficient heat transfer route is built for the high heat flux from the hotspot.

TABLE I. GEOMETRIC PARAMETERS

Parameter	*Symbol*	*Value*
Inlet diameter	d_{in}	100 µm
Outlet diameter	d_{out}	100 µm
Unit cell length	L_{unit}	600 µm
Cavity height	h_{cav}	100 µm
Silicon layer height	h_{Si}	105 µm
TSV height	h_{TSV}	100 µm
TSV diameter	d_{TSV}	0~600 µm
Hotspot length	L_{hs}	100 µm

For CFD simulation, a unit cell model is taken out from the nozzle array to reduce the computational time. As shown in Fig. 1c, the cross-sectional view indicates that the unit cell model contains a single inlet nozzle and four one-fourth outlet nozzles. The configuration of the unit cell model is defined by several geometric parameters, including parameters of the fluid domain and dimensions of the solid domain. The fluid domain is described by the parameters of the nozzle array, including inlet diameter d_{in}, outlet diameter d_{out}, unit cell length L_{unit}, and cavity height h_{cav}. While the solid domain, including the silicon die and copper TSV, is defined by silicon layer height h_{Si}, TSV height h_{TSV}, and TSV diameter d_{TSV}. A square shape hotspot with a length of L_{hs} is applied to benchmark the cooling performance of the design. A high heat flux of q_{hs}"=600 W/cm^2 is assumed to be generated in the hotspot region, and a background heat flux of q_{bg}"=20 W/cm^2 is specified for all other areas on the chip heat source regions. The values of the geometric parameters are listed in Table I.

B. Simulation Method

Ansys 2022R2 platform is used in this work to perform conjugate heat transfer and fluid dynamics simulation, which considers both the convection by the impingement jet and the conduction in the silicon layer. The unit cell model is used to simulate the heat transfer characteristics. Previous works have demonstrated that the effects of cooler structure materials on the heat transfer characteristics of the cooler can be neglected [18]. Therefore, the computational domain only contains a fluid region of flow in the cavity and nozzles and a solid region of the die.

The turbulence model is chosen based on the evaluation of the inlet Reynolds number

$$\mathrm{Re}_{in}=U_{in}d_{in}/\nu \quad (1)$$

where ν is the kinematic viscosity of the fluid. In this work, the inlet velocity and inlet temperature are chosen as U_{in}=3 m/s and T_{in}=300 K for all the simulations, resulting in an inlet Reynolds number of Re_{in}=299. Considering that the reported turbulence transition range of the impingement jet is Re_{in}=1000~3000 [19], the laminar model is used here for simulating the fluid dynamics of the impingement jet. The Semi-implicit method for Pressure-linked Equations (SIMPLE) algorithm with Quadratic Upstream Interpolation for Convective Kinematics (QUICK) scheme is applied to solve the Navier–Stokes equations.

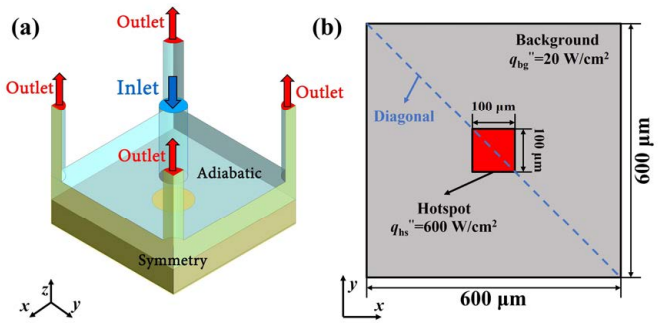

Fig. 2. Boundary conditions of the unit cell model. (a) All side surfaces are set as symmetric boundaries. The interfaces between the fluid domain and the cooler are assumed to be adiabatic. (b) Power map of the chip interface. A square hotspot with a high heat flux of q_{hs}"=600 W/cm^2 is used for the benchmark. The Blue dotted line represents the diagonal direction.

As shown in Fig. 2, boundary conditions are set up based on the physical properties of different boundaries. All the fluid-solid interfaces are assumed to be no-slip surfaces, indicating that the relative velocity between fluid and solid is zero at interfaces. The fluid inlet is set as a uniform velocity inlet and outlets are set as pressure outlets with a gauge pressure of 0 Pa. As shown in Fig. 2a, Symmetric boundary conditions are specified for all the side surfaces of the unit cell model to simulate the fluid dynamics of the impingement jet from a nozzle array, and the interfaces between fluid and the cooler materials are set as adiabatic boundaries as the heat transferred to the cooler materials is negligible [18]. As mentioned above, the heat dissipation of the chip is characterized by a non-uniform heat flux distribution with a hotspot region and a background region. Fig. 2b shows the power map of the chip interface, which defines the heat flux boundary conditions on the bottom surface of the unit cell model.

As shown in Fig. 3, the detailed geometry of the model is described by fine meshing with a maximum mesh size of 5 µm. Hybrid meshing is chosen, which uses prism mesh to capture boundary layer features and generates tetrahedral mesh cells to describe the dynamics of other fluid domains. The meshing of thermal TSV is refined at small TSV diameters to ensure

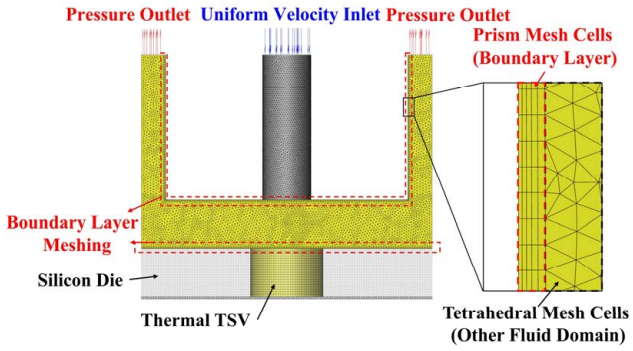

Fig. 3. Meshing of the unit cell model with a maximum mesh size of 5 µm. Denser prism mesh cells are applied near the liquid-solid interfaces to capture the boundary layer flow.

accuracy. The mesh sensitivity is analyzed by comparing the temperature rise at maximum mesh sizes of 5 μm and 2.5 μm. The relative deviation of temperature rise is 0.46%, indicating that the current mesh size of 5 μm fulfills the requirement of mesh independence.

C. Parameters Extraction

The cooling performance of the design is assessed from two different aspects: maximum temperature and temperature uniformity. As shown in Fig. 4, the maximum temperature $T_{\text{bot,max}}$ is defined as the temperature of the hottest point on the bottom surface, which is usually located at the center of the hotspot region. A thermal resistance network is sketched in Fig. 4, which consists of the maximum spreading resistance, 1D conduction resistance, and convection resistance. The maximum temperature is normalized as the overall thermal resistance per unit area to allow comparison between different cooling solutions.

$$R_{\text{tot}} = \frac{T_{\text{bot,max}} - T_{\text{in}}}{q''_{\text{bg}} A_{\text{bg}} + q''_{\text{hs}} A_{\text{hs}}} A_{\text{chip}} \tag{2}$$

where A_{hs}, A_{bg}, and A_{chip} denote the area of the hotspot region, background region, and the entire chip interface, respectively.

Temperature uniformity is predominantly affected by the heat flux distribution on the chip interface. Sharma et al. [3] have introduced a normalized temperature difference to enable comparison between scenarios with different levels of heat flux non-uniformity. In their definition, the temperature difference between the maximum and minimum temperature on the chip interface is normalized by the ratio of hotspot heat flux to background heat flux. The normalized temperature difference is adopted here to characterize the temperature uniformity of the chip interface.

$$\Delta T_{\text{q}} = \frac{T_{\text{bot,max}} - T_{\text{bot,min}}}{q''_{\text{hs}} / q''_{\text{bg}}} \tag{3}$$

where $T_{\text{bot,min}}$ is the minimum temperature on the chip interface.

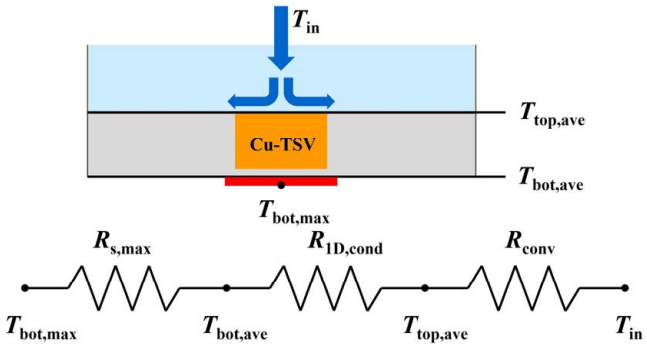

Fig. 4. Definitions of different temperatures and a thermal resistance network that includes spreading, 1D conduction, and convection thermal resistances.

Heat spreading is another important consideration in the design of cooling solutions for microelectronics. It is often characterized by thermal spreading resistance $R_{\text{s, max}}$, which is defined by the temperature difference between the maximum and average temperature of the heat flux surface.

$$R_{\text{s,max}} = \frac{T_{\text{bot,max}} - T_{\text{bot,ave}}}{q''_{\text{bg}} A_{\text{bg}} + q''_{\text{hs}} A_{\text{hs}}} A_{\text{chip}} \tag{4}$$

where $T_{\text{bot,ave}}$ is the average temperature of the bottom surface. A large thermal spreading resistance indicates a high peak temperature and a non-uniform temperature distribution. Therefore, the suppression of heat spreading is often desired in hotspot-targeted cooling solutions.

III. Results and Discussion

A. Effects of TSV Diameter

A circular thermal TSV with a diameter of d_{TSV}=100 μm is first integrated with jet impingement cooling and benchmarked by comparison with different cooling schemes. The total thermal resistance and normalized temperature difference are calculated and compared in four cooling solutions:

(1) Conventional cooling solution (Uniform HTC).
(2) Conventional cooling solution with thermal TSV (TSV only).
(3) Impingement jet cooling solution (Jet only).
(4) Impingement jet cooling solution with thermal TSV (Jet+TSV).

To allow a fair comparison, the effective convective HTC in conventional cooling solutions is set the same as the average HTC in jet cooling solutions.

The overall thermal resistance and normalized temperature difference calculated from CFD simulations are shown in Fig. 5. The results indicate that compared to conventional cooling solutions with uniform HTC, both jet impingement cooling and thermal TSV decrease the peak temperature and increase the temperature uniformity. The jet impingement cooling shows a

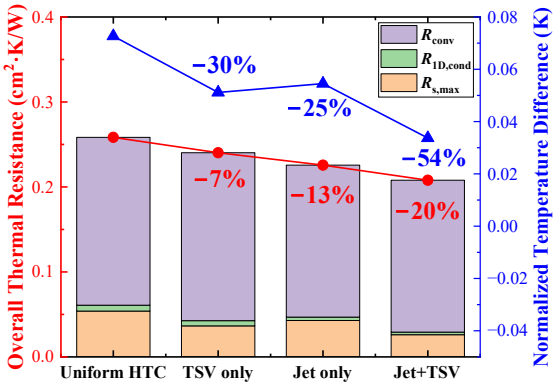

Fig. 5. Comparison of overall thermal resistance and normalized temperature uniformity in different cooling solutions. The hybrid jet impingement/thermal TSV cooling scheme shows the lowest overall thermal resistance and normalized temperature difference.

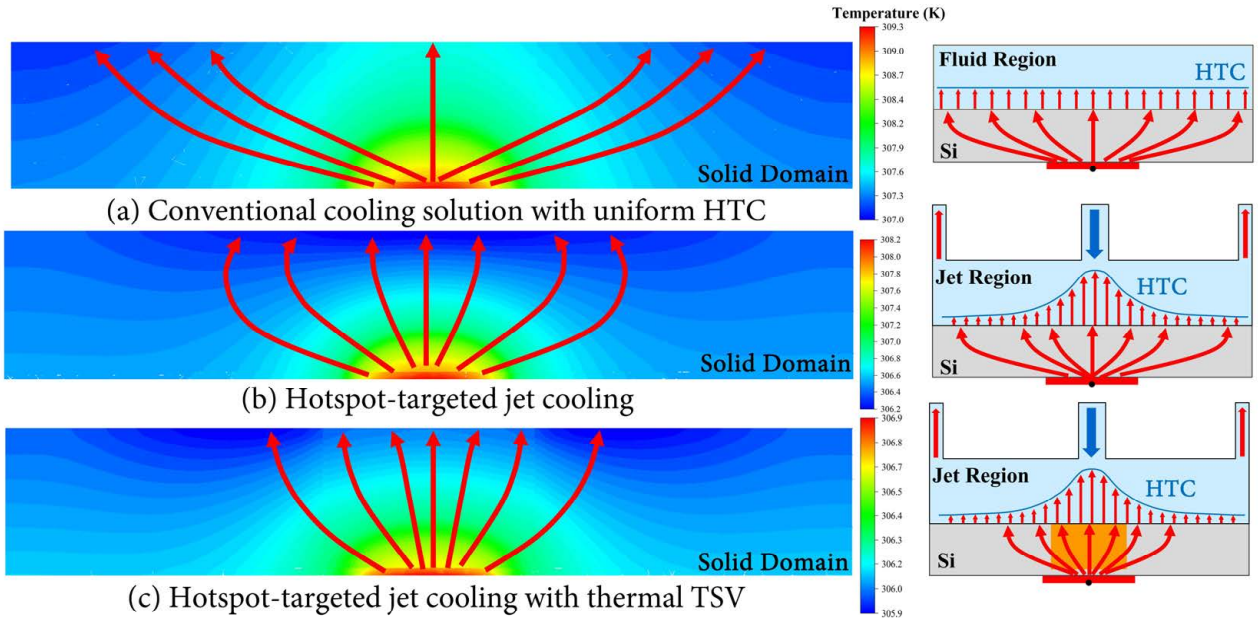

Fig. 6. Comparison between cross-sectional temperature profiles of the solid layer in different cooling schemes. (a) Conventional cooling solution with uniform HTC distribution on the top surface. (b) Hotspot-targeted jet impingement cooling solution with an HTC peak at the nozzle center. (c) Hotspot-targeted jet cooling with copper thermal TSV.

better performance in reducing overall thermal resistance while thermal TSV exhibits a larger decrease in normalized temperature difference. The hybrid cooling solution integrates thermal TSV with jet impingement cooling and thus combines the advantages of both sides to make a cooling solution with the lowest peak temperature and best temperature uniformity. Moreover, it is noted that the 1D conduction resistance shows some difference between cooling solutions. However, the 1D conduction resistance only accounts for a very small part of the total thermal resistance and may only have limited numerical accuracy due to the extremely small temperature difference between the bottom and top surface of the solid domain (~0.1 K). Therefore, the discussion on the variation of 1D conduction resistance may not be meaningful and is not included here.

The mechanisms behind the superior cooling performance of the hybrid jet impingement/thermal TSV cooling scheme can be explained by analyzing heat spreading in the solid layer. As shown in Fig. 6, the cross-sectional temperature profile of the solid layer is plotted for different cooling solutions. In a conventional cooling scheme, the uniform HTC distribution on the top surface results in significant heat spreading. The high heat flux in the hotspot region spreads to the whole top surface and thus generates a large spreading resistance, which increases the overall thermal resistance and decreases the temperature uniformity. With a non-uniform HTC generated by jet impingement, the heat flux first spreads and then shrinks toward the high-HTC stagnation region near the nozzle region, which confines the heat spreading to some extent. In addition, compared to the conventional cooling solution, as more heat flux is concentrated and dissipated in the high-HTC region, the effective HTC is increased, leading to a lower convection thermal resistance. Applying a thermal TSV can further suppress heat spreading as the higher thermal conductivity of copper TSV than the silicon layer considerably restricts the horizontal spreading of heat flux from copper to silicon. Thus, the hybrid jet impingement/thermal TSV cooling shows a minimum heat spreading and the lowest overall thermal resistance.

As thermal TSVs with large volumes occupy valuable space for signal routing and may bring about fabrication challenges, one of the most important design objectives in this hybrid cooling scheme is to minimize the material usage or volume of the thermal TSV. The cooling performance of circular thermal TSVs with different diameters is first evaluated to study the effects of TSV dimensions. Fig. 7 shows the overall thermal resistances and normalized temperature differences at different diameters of thermal TSV. The results indicate that, with the enlargement of thermal TSV, both the peak temperature and temperature uniformity first decrease rapidly and then more slowly after reaching d_1=100 μm. When the TSV diameter exceeds d_2=300 μm, the overall thermal resistance remains almost invariant, and the normalized temperature difference shows a gentle increase with the TSV diameter.

As shown in Fig. 7, the variation of cooling performance with TSV diameter can be divided into three regimes according to the changing trends. Three different TSV diameters are selected from the three regimes respectively. The temperature distribution is plotted along the diagonal direction of the chip interface (blue dotted line in Fig. 2b) and compared at different TSV diameters, as shown in Fig. 8.

In the first regime, the cross-section of thermal TSV stays inside the hotspot region. Fig. 8 shows that as the thermal TSV cannot cover the whole hotspot region, the temperature distribution shows a sudden drop at the center due to the transition to the TSV region. In this regime, with TSV diameter increases, more area of the hotspot region is overlapped with

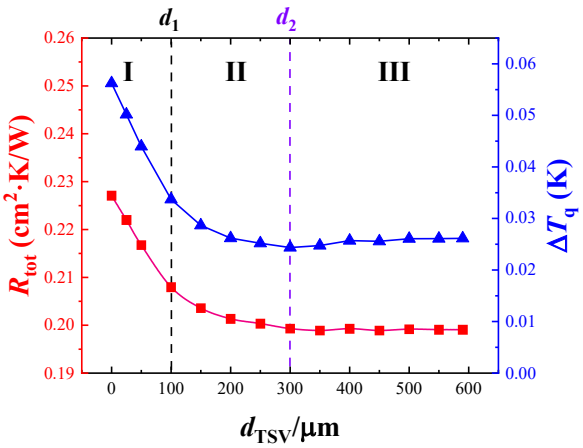

Fig. 7. Variation of overall thermal resistance and normalized temperature difference with TSV diameter.

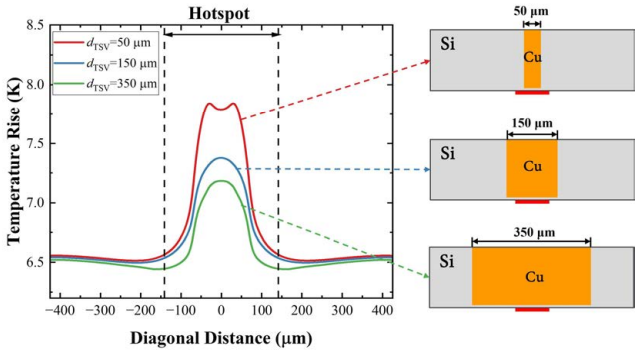

Fig. 8. Diagonal temperature distribution on the chip interface at different TSV diameters. The temperature rise is defined as the difference between inlet temperature and chip temperature.

the copper TSV. The thermal TSV is able to cover a larger fraction of hotspot heat flux, resulting in a more predominant suppression of heat spreading and better temperature uniformity. Besides, the enlargement of thermal TSV also contributes to the reduction of overall thermal resistance by decreasing the 1D conduction resistance with lower effective thermal conductivity.

In regime II, although the large thermal TSV restricts the heat spreading from TSV to the surrounding silicon layer, the hotspot heat flux can spread in the bulk of copper TSV as the size of the TSV becomes larger than the hotspot region. The heat spreading in copper TSV increases the spreading resistance and adversely impacts the temperature uniformity. Nevertheless, the benefits of confining copper-to-silicon heat fluxes still overweight the heat-spreading effects in bulk copper, resulting in a gentle enhancement of cooling performance with the enlargement of TSV.

As TSV diameter approaches regime III, the heat spreading in copper TSV becomes dominant and eliminates the benefits of TSV on spreading resistance. The spreading resistance starts to increase with the TSV diameter, leading to a larger temperature difference. In this regime, even though TSV enlargement can still decrease the 1D conduction resistance, it will be neutralized by the increasing spreading resistance, causing an almost invariant overall thermal resistance. As shown in Fig. 8, compared with thermal TSV in regime II (d_{TSV}=150 μm), the thermal TSV in regime III (d_{TSV}=350 μm) shows a lower peak temperature due to a reduced overall thermal resistance. However, a lower minimum temperature is also found in the case of d_{TSV}=350 μm, illustrating that the heat spreading in thermal TSV adversely affects the temperature uniformity.

B. *Effects of TSV Shape*

Another design factor that might affect the thermal performance of the design is the cross-sectional shape of thermal TSV, which can be modified by lithography during the fabrication process. We first evaluated and compared the cooling performance of thermal TSVs with circular and square cross-sections. As shown in Fig. 9, the normalized temperature difference and overall thermal resistance of square TSV are both very close to that of circular TSV under the same cross-sectional areas. According to the results, we can assume that the cross-sectional shape only has minimal influence on the performance of the hybrid cooling solution.

To further verify our assumption, we have performed CFD simulations to assess the performance of TSVs with different shapes. In addition to the circular and square TSVs, TSVs with a diamond-shaped cross-section and a star-shaped cross-section are tested. As shown in Fig. 10, the diagonal temperature profile of the chip interface is plotted for TSVs with different shapes and the same cross-sectional area. The results illustrate that no significant difference is observed between them, which demonstrates our assumption that the cooling performance mainly depends on the TSV cross-sectional area instead of the shape.

C. *Effects of TSV Density*

Although the hybrid jet impingement/ thermal TSV cooling solution can enhance temperature uniformity, there is still an obvious temperature rise in the hotspot region due to the mismatch between the HTC distribution and heat flux distribution. The heat flux in the hotspot region can achieve ~30 times higher than the background heat flux [20], requiring the same multiplication of effective HTC in the hotspot region to

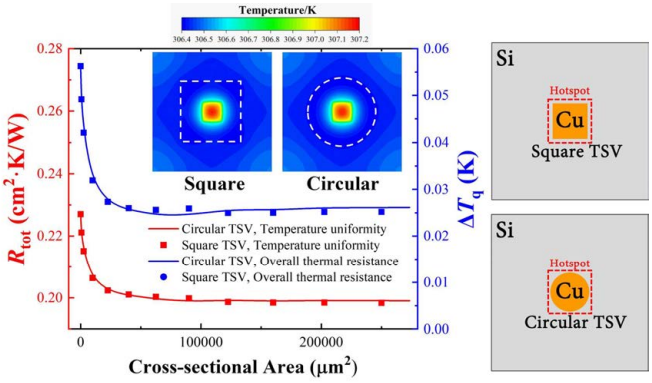

Fig. 9. Comparison between circular and square TSV. Solid lines and dots represent the simulated values of circular and square TSV, respectively.

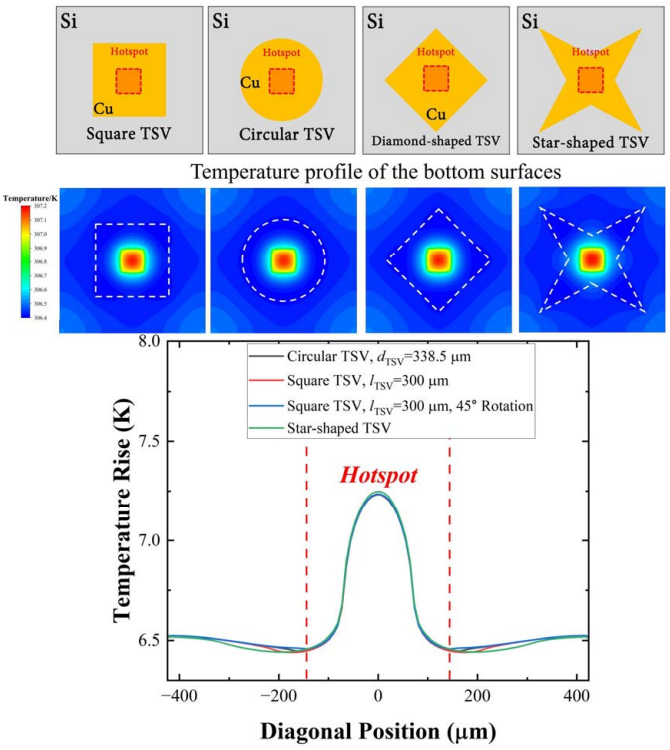

Fig. 10. Diagonal temperature distribution for TSVs with different shapes and the same cross-sectional area.

achieve an ideally uniform temperature distribution. However, the HTC of the stagnation region is typically less than 10 times larger than that in the wall jet region in conventional jet cooling schemes [15].

Several surface enhancement methods have been proposed to increase the effective HTC by strengthening the convective heat transfer in the hotspot region, such as the application of porous media and silicon micro-fins on the die surface [12], [13]. Here, we present an idea that fabricates an array of TSVs near the hotspots and exposes them to the impingement jet by etching the silicon layer as shown in Fig. 11. Our design utilizes the exposed TSV array as micro-fins to enhance convective heat transfer in the hotspot region, which combines surface enhancements with thermal TSVs to further strengthen the heat dissipation from hotspots. Compared to silicon micro-fins, thermal TSVs are made of metal materials with high thermal conductivities and thus have higher fin efficiency. Moreover, this design eases the fabrication process as thermal TSVs and micro-fins are manufactured simultaneously by a TSV fabrication process followed by silicon etching. It is also worth noting that thinning the silicon substrate can change the spreading and conduction resistance and thus affects the thermal performance. However, compared to the predominant effects of convective heat transfer enhancement brought about by the exposed TSVs, silicon thinning only has minor effects. Moreover, the spreading resistance varies distinctively with the substrate thickness at different conditions [21], causing difficulty for qualitative analysis, especially for the complicated system proposed here.

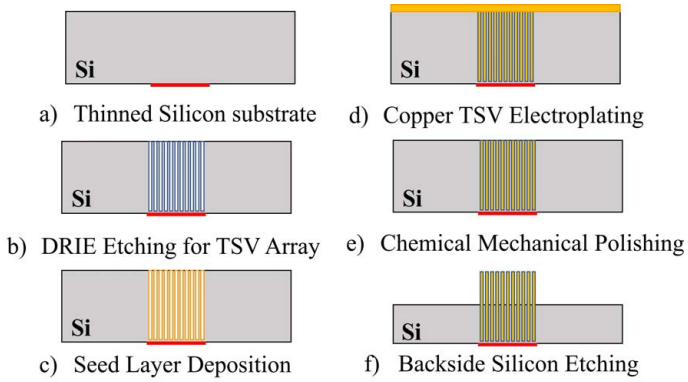

Fig. 11. Fabrication process of exposed TSV array. (a) Thinned silicon substrate. (b) An array of vias is fabricated in silicon by DRIE etching. (c) A copper seed layer is deposited by physical vapor deposition (PVD). (d) Bottom-up electroplating of copper TSVs. (e) Excessive copper is polished by chemical mechanical polishing (CMP). (f) The TSV array is exposed by the backside etching of the silicon layer.

The cooling performance of the exposed TSV array is benchmarked by comparison with the buried TSV array and a single TSV with the same cross-sectional area. 11×11 TSVs with a diameter of d_{TSV}=5 μm are regularly arranged in the hotspot region to form an array. The surrounding silicon layer is etched 50 μm for exposing the TSV array to the impingement jet. As shown in Fig. 12, the diagonal temperature distribution on the chip interface is calculated for different cases. The results illustrate that either exposing the single TSV or TSV array leads to a lower peak temperature while the exposed TSV array remarkably increases the temperature uniformity. Among the four cases, the scheme with the exposed TSV array shows the best cooling performance, illustrating a significant improvement compared to either single TSVs or the buried TSV array.

Moreover, the effects of Si thinning are analyzed as the Si thickness can vary the length of the exposed part of the TSV array and also influence the spreading and 1D conduction resistances in the solid domain. CFD simulations are performed for exposed TSV arrays with different Si thicknesses, which is denoted as t_{Si} here. As shown in Fig. 13, the difference between maximum and minimum temperature keeps decreasing with the decreased Si thickness, indicating better temperature uniformity at low Si thicknesses. The temperature peak also monotonically decreases with the decrease in Si thickness, showing a reduction in total thermal resistance. The better temperature uniformity and lower total thermal resistance can be attributed to the effect of thinning the silicon layer. Si thinning enhances the convective heat transfer by exposing more TSV array and also reduces the 1D conduction resistance by decreasing the thickness of the solid domain, leading to a better cooling performance of the TSV array. Besides, the Si thinning should also have effects on heat spreading. However, due to the complexity of the system and the different changing trends of spreading resistance at different conditions [21], the effects of Si thickness on the spreading resistance are hard to analyze and need further in-depth studies. It is also worth noting that the average temperature at t_{Si}=25 μm is apparently larger than at t_{Si}=50 μm, which is assumed to be attributed to the large distance between

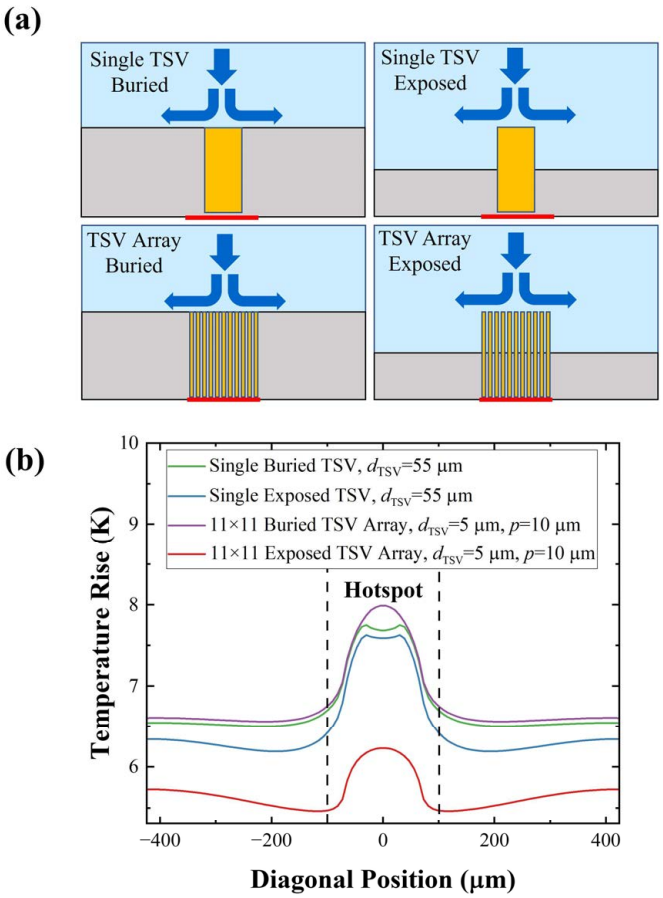

Fig. 12. Comparison between buried and exposed single TSVs and TSV arrays. The cross-sectional area is kept the same for all four cases. (a) Schematics of different thermal TSVs. (b) Diagonal temperature profile. The cooling solution with an exposed TSV array shows the lowest temperature peak and best temperature uniformity.

the silicon substrate and the impingement point of the jet (at the top of the TSV array) due to Si thinning.

Furthermore, the exposed TSV arrays with different array densities are investigated as the density of the TSV array can affect both the heat transfer and flow characteristics of the cooling solution. It can be predicted that as the TSV array becomes denser, the total surface area of the micro-fins increases and thus facilitates the convective heat transfer. However, the gap between the TSVs is reduced at large array densities, resulting in huge flow resistance in the microchannels between TSVs. The increased flow resistance hinders the impingement jet from flowing into the TSV array, leading to a strong bypass flow, and adversely impacting the heat transfer between TSVs and fluids. The simulated flow velocity distribution on the cross-sections of the TSV arrays is shown in Fig. 14. Compared to a 5×5 TSV array where the maximum velocity appears inside the TSV array, the flow field near the 11×11 TSV array is similar to the case with a single TSV, where the mass flow rate concentrates near the side surfaces of the TSV array, indicating a dominant bypass flow. For an 11×11 TSV array, although there is still some fluid that can flow through the TSV array, especially in the top part of the array, the enlargement of the

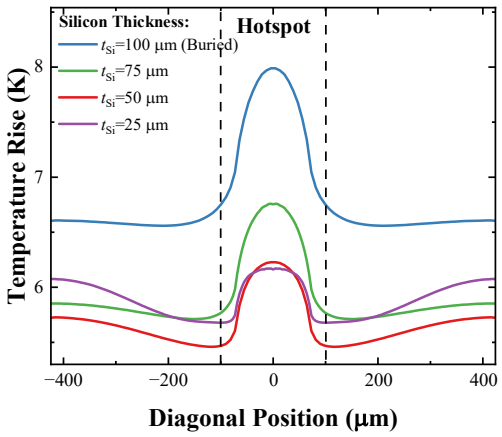

Fig. 13. Comparison of the temperature profile at different Si thicknesses. Both the peak temperature and the temperature difference decrease with the decreasing Si thickness.

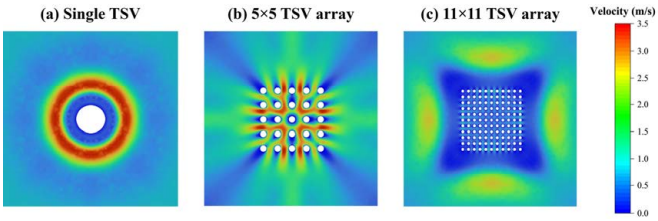

Fig. 14. Velocity profile of fluids on the cross-sections of TSV arrays with different densities. (a) Single TSV with d_{TSV}=55 μm. (b) 5×5 TSV array with d_{TSV}=11 μm. (c) 11×11 TSV array with d_{TSV}=5 μm.

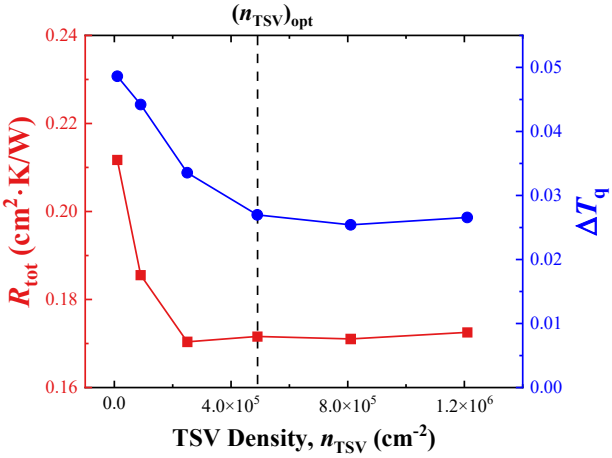

Fig. 15. Overall thermal resistance and normalized temperature difference at different TSV densities. Increasing TSV density shows no benefits at n_{TSV}>4.9×10^5 cm^{-2}.

total surface area fails to eliminate the bypass effect, hindering the continuing enhancement of the cooling performance with TSV density.

As shown in Fig. 15, the peak temperature and temperature difference first rapidly decreases with the array density due to the enlargement of the total surface area. After the density exceeds $(n_{TSV})_{opt}$=4.9×10^5 cm^{-2}, a denser TSV array shows no

significant benefit on the cooling performance due to the dominant effects of increasing flow resistance in the TSV array. The simulation results are in good agreement with our predictions.

In addition, considering that the array density can affect the flow characteristics of the impingement jet, we also evaluated the system pressure drop at different TSV densities. The difference between the inlet and outlet pressure is defined as the pressure drop. The pressure drop is calculated at all the studied TSV densities. The results show that the pressure drop values are all in the range of 20.28 kPa ~20.41 kPa, and the relative variation is less than 0.4%, indicating that the effect of array density on the pressure drop is negligible.

IV. Conclusions

In this paper, a hybrid jet impingement/ thermal TSV cooling scheme is proposed to eliminate hotspots on chips. CFD simulations are performed to benchmark the cooling performance of the scheme by comparing it with three other reference cooling solutions. The effects of TSV diameter and cross-sectional shape are investigated to achieve an optimal design with minimum routing space occupied. Moreover, a design with an exposed TSV array is presented, which utilized the TSV array as a surface enhancement to further increase the cooling performance. The effects of TSV array density are investigated. The main conclusions are as follows.

(1) The proposed cooling solution combines the superior heat conduction of thermal TSV and the strong convection in the stagnation region of the impingement jet to facilitate heat dissipation from hotspots. Compared to other cooling solutions, the proposed solution shows both a significant improvement in temperature uniformity and a remarkable reduction of overall thermal resistance.

(2) As the TSV diameter increases, both the peak temperature and temperature difference first decrease rapidly and then remain almost invariant after reaching a critical diameter. The excessive enlargement of thermal TSV brings about no benefits due to the stronger heat spreading in the bulk of TSV. The cooling performance of the solution mainly depends on the cross-sectional area instead of the shape of the TSV.

(3) The effective HTC can be further increased by fabricating an array of TSVs in the hotspot region and exposing TSVs to the impingement jet by etching the surrounding silicon layer. The simulation results indicate that the exposed TSV array remarkably enhances the convective heat transfer and improves the cooling performance. As the array density increases, the total surface area of TSVs is enlarged while the flow resistance in the array is increased, rendering an optimal value of array density.

References

[1] R. van Erp, R. Soleimanzadeh, L. Nela, G. Kampitsis, and E. Matioli, "Co-designing electronics with microfluidics for more sustainable cooling," Nature 2020 585:7824, vol. 585, no. 7824, pp. 211–216, Sep. 2020.

[2] A. Bar-Cohen and P. Wang, "Thermal management of on-chip hot spot," J. Heat Transfer, vol. 134, no. 5, May 2012.

[3] C. S. Sharma et al., "Energy efficient hotspot-targeted embedded liquid cooling of electronics," Appl. Energy, vol. 138, pp. 414–422, Jan. 2015.

[4] S. B. Riffat and X. Ma, "Improving the coefficient of performance of thermoelectric cooling systems: a review," Int. J. Energy Res., vol. 28, no. 9, pp. 753–768, Jul. 2004.

[5] J. Qu, H. Wu, P. Cheng, Q. Wang, and Q. Sun, "Recent advances in MEMS-based micro heat pipes," Int. J. Heat Mass Transf., vol. 110, pp. 294–313, Jul. 2017.

[6] Z. Gao, Y. Zhang, Y. Fu, M. M. F. Yuen, and J. Liu, "Thermal chemical vapor deposition grown graphene heat spreader for thermal management of hot spots," Carbon, vol. 61, pp. 342–348, Sep. 2013.

[7] Y. Han, B. L. Lau, G. Tang, and X. Zhang, "Thermal management of hotspots using diamond heat spreader on si microcooler for GaN devices," IEEE Trans. Compon. Packaging Manuf. Technol., vol. 5, no. 12, pp. 1740–1746, Dec. 2015.

[8] P. Y. Paik, V. K. Pamula, and K. Chakrabarty, "A digital-microfluidic approach to chip cooling," IEEE Design and Test of Computers, vol. 25, no. 4, pp. 372–391, 2008.

[9] C. S. Sharma, M. K. Tiwari, and D. Poulikakos, "A simplified approach to hotspot alleviation in microprocessors," Appl. Therm. Eng., vol. 93, pp. 1314–1323, Jan. 2016.

[10] T. Wei et al., "Numerical Study of Large Footprint (24 × 24 mm2) Silicon-Based Embedded Microchannel Three-Dimensional Manifold Coolers," J. Electron. Packag., vol. 145, no. 2, Jun. 2023.

[11] T. Wei, H. Oprins, V. Cherman, E. Beyne, and M. Baelmans, "Low-Cost Energy-Efficient On-Chip Hotspot Targeted Microjet Cooling for High-Power Electronics," IEEE Trans. Compon. Packaging Manuf. Technol., vol. 10, no. 4, pp. 577–589, Apr. 2020.

[12] Z. Soleymani, M. Rahimi, M. Gorzin, and Y. Pahamli, "Performance analysis of hotspot using geometrical and operational parameters of a microchannel pin-fin hybrid heat sink," Int. J. Heat Mass Transf., vol. 159, p. 120141, Oct. 2020.

[13] E. Farsad, S. P. Abbasi, and M. S. Zabihi, "Fluid flow and heat transfer in a novel microchannel heat sink partially filled with metal foam medium," J. Therm. Sci. Eng. Appl., vol. 6, no. 2, Jan. 2014.

[14] P. Łapka, A. Ciepliński, and A. Rusowicz, "Numerical model and analysis of heat transfer during microjets array impingement," Energy, vol. 203, p. 117879, Jul. 2020.

[15] S. V. Garimella, "HEAT TRANSFER AND FLOW FIELDS IN CONFINED JET IMPINGEMENT," Annual Review of Heat Transfer, vol. 11, no. 11, pp. 413–494, Mar. 2000.

[16] Z. Ren, A. Alqahtani, N. Bagherzadeh, and J. Lee, "Thermal TSV Optimization and Hierarchical Floorplanning for 3-D Integrated Circuits," IEEE Trans. Compon. Packaging Manuf. Technol., vol. 10, no. 4, pp. 599–610, Apr. 2020.

[17] B. Goplen and S. S. Sapatnekar, "Placement of thermal vias in 3-D ICs using various thermal objectives," IEEE Transactions on Computer-Aided Design of Integrated Circuits and Systems, vol. 25, no. 4, pp. 692–708, Apr. 2006.

[18] T. Wei et al., "High efficiency direct liquid jet impingement cooling of high power devices using a 3D-shaped polymer cooler," Technical Digest - International Electron Devices Meeting, IEDM, pp. 32.5.1-32.5.4, Jan. 2018.

[19] N. Zuckerman and N. Lior, "Jet Impingement Heat Transfer: Physics, Correlations, and Numerical Modeling," Adv. Heat. Transf., vol. 39, no. C, pp. 565–631, Jan. 2006.

[20] K. P. Drummond et al., "Characterization of hierarchical manifold microchannel heat sink arrays under simultaneous background and hotspot heating conditions," Int. J. Heat Mass Transf., vol. 126, pp. 1289–1301, Nov. 2018.

[21] M. W. Denhoff, "An accurate calculation of spreading resistance," J. Phys. D: Appl. Phys., vol. 39, no. 9, pp. 1761–1765, Apr. 2006.